

# Emergence of a giant rotating cluster of fish in three dimensions by local interactions

Susumu Ito and Nariya Uchida\*

*Department of Physics, Tohoku University, Sendai, 980-8578, Japan*

(Dated: January 11, 2022)

Schooling fish exhibit giant rotating clusters such as balls, tori, and rings, among other collective patterns. In order to account for their giantness and flexible shape change, we introduce an agent-based model that limits the number of agents that each agent can interact with (interaction capacity). Incorporating autonomous control of attractive interaction, we reproduce rotating clusters that are an order of magnitude larger than the interaction range. We obtained a phase diagram of patterns including polarized schools and swarms. The model indicates that giant rotating clusters are formed at low interaction capacity, without long-range interactions or inherent chirality of fish.

*Introduction.* Cluster formation and collective motion are ubiquitously found in life of various organisms [1–3]. Moving clusters are classified into “swarms” of randomly oriented individuals, “polarized schools” with directed movement, and “vortices” or rotating clusters [4]. Schooling fish exhibit giant vortices (balls, tori, and rings) [5–9], which sometimes contain several thousands of fish and have a diameter of several ten times the body length [8]. Compared to vortices in other biological systems, where rotational symmetry is broken by inherent chirality of the basic element [10, 11] or by interaction with boundaries [12, 13], vortices of fish are unique and highly non-trivial in that the symmetry is spontaneously broken only by interaction between the moving elements [14].

Previous models of fish schools are based on agent-based approach [15–18]. Vortices are induced by combination of isotropic attraction and repulsion [19–22], or asymmetrical interaction via a viewing angle [23–29]. However, models with short-range interactions reproduce small vortices with their radii shorter than the interaction range. An alternative approach is metric-free models that limit the number of neighbors to interact by a constant (“topological interaction”) or Voronoi tessellation [30, 31]. The topological interaction was originally introduced for flocks of birds [32–35]. It enables a cluster to sensitively reacts on the motion of a small number of agents, such as those attacked by a predator, and to flexibly change its shape. However, metric-free interactions also do not reproduce giant vortices of fish, and it is proposed that [36] long-range hydrodynamic interaction is necessary to correctly describe sizable vortices. These results strengthen the view that direct interactions between all or most of the agents in a cluster is the requisite to cause spontaneous breaking of rotational symmetry. (See Supplemental Material for detailed discussions of the previous studies.)

In this Letter, we overturn the pervading view and propose a new mechanism of spontaneous symmetry breaking that requires only local interactions to form giant vortices. Here, “giant” means that the cluster size is much

larger than the radius of interaction. The key idea is to limit the neighbors to interact by both their number and distance. Limiting the maximum number of neighbors that each fish can interact with (which we call “interaction capacity”) is necessary to avoid the attractive interactions to pile up and induce unphysically dense clusters. In fact, there is an experimental evidence that attraction is weakened in a cluster of fish [37]. Experiments also show that the attraction and repulsion are balanced at a fixed distance for a pair of fish outside the cluster [37, 38]. Therefore, we combine the interaction capacity and fixed range of interaction in our model. On the other hand, it is also suggested that fish use asymmetrical interaction via a blind angle [37, 38]. Theoretically, many previous models [24–29, 31] show that introducing the blind angle promotes formation of a rotating cluster. However, we do not consider the blind angle in our model in order to focus on the effect of interaction capacity, and show that we can still obtain rotating clusters.

*Model.* The model is based on experimentally observed behaviors of fish. First, attractive interaction is balanced with repulsive interaction at the equilibrium distance  $r_e$  for a few fish, but is weakened in a cluster (while repulsion within  $r_e$  remains). Secondly, it is observed for three different species of fish that up to the third nearest neighbors are distributed within 1.5 body lengths (BL) from each fish [39]. This distance is close to the value of  $r_e$  obtained in Refs. [37, 38], which implies that the interaction capacity of some fish is a few. Finally, we take notice of an acceleration mode of fish to escape from predators called “fast-start” [40–42]. Some fish in a cluster change their velocity by swimming away from predators, and the change propagates to other fish and causes a dynamic shape change of the cluster [43–45]. Fast-start has duration of about 0.1 sec [46, 47]. We model this by turning on attraction when a fish is located outside a cluster and has only a small number of neighbors within  $r_e$ . The attraction lasts for duration  $\tau$  and helps the fish unite with the cluster, which we regard equivalent to escaping from a (hypothetical) predator. Note that an experiment shows that fish also have orientational interaction [48]. Integrating these properties, we formulate the model as follows.

We consider  $N$  agents moving in a cubic box of size  $L$  with the periodic boundary condition. Let  $\mathbf{r}_i$  and

---

\* uchida@cmpt.phys.tohoku.ac.jp

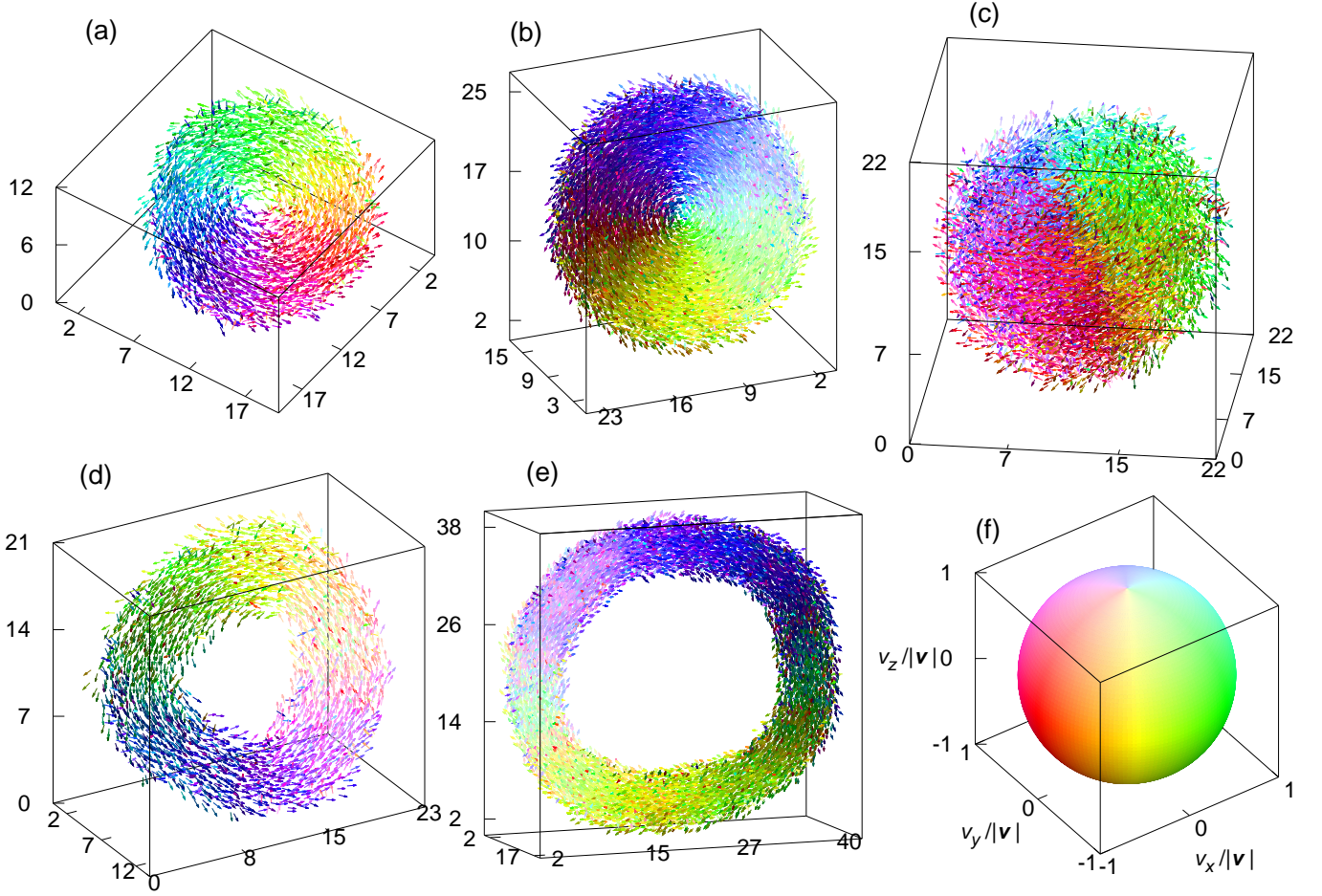


FIG. 1. Snapshots of fish clusters. Agents are represented by arrows of length  $2/3$  ( $=1$  BL), and the color corresponds to the moving direction of the agent according to the color sphere (f). Shown are only a small part of the simulation box that contains the agents and the origin is shifted for visibility. (a) A torus for  $N = 3000$ ,  $N_u = 3$ ,  $\lambda = 7.0$ . (b) A torus for  $N = 10000$ ,  $N_u = 3$ ,  $\lambda = 11.0$ . (c) A rotating ball for  $N = 10000$ ,  $N_u = 1$ ,  $\lambda = 11.0$ . (d) A ring for  $N = 3000$ ,  $N_u = 3$ ,  $\lambda = 4.5$ . (e) A ring for  $N = 10000$ ,  $N_u = 3$ ,  $\lambda = 7.0$ . (f) The color sphere corresponding to agent's direction  $\mathbf{v}/|\mathbf{v}| = (v_x/|\mathbf{v}|, v_y/|\mathbf{v}|, v_z/|\mathbf{v}|)$ . It is a pure hue on the plane of  $v_z/|\mathbf{v}| = 0$ , and whitish hue when  $v_z/|\mathbf{v}| > 0$  and blackish hue when  $v_z/|\mathbf{v}| < 0$ . See Movie S1-S5 for dynamics.

$\mathbf{v}_i = d\mathbf{r}_i/dt$  ( $i = 1, 2, \dots, N$ ) be the position and velocity of the  $i$ -th agent, respectively. The velocity is set to relax to the sustained speed  $v_0$  for an isolated agent, and is modified by orientational, repulsive, and attractive interactions (fast-start) with the neighbor agents. The orientational and repulsive interactions act with up to  $N_u$ -th nearest neighbors in the radius  $r_e$ , where  $N_u$  is the interaction capacity. The set of agents that can interact with the  $i$ -th agent by orientational and repulsive interactions is denoted by  $\mathcal{L}_i$ , and the number of them by  $|\mathcal{L}_i|$ . The “occupancy ratio”  $\eta_i = |\mathcal{L}_i|/N_u$  is less than or equal to unity and shows how much of the interaction capacity is used. The attractive interaction operates at distances between  $r_e$  and  $r_a$ , and the set of agents that can attract the  $i$ -th agent is denoted by  $\mathcal{A}_i = \{j | r_e < |\mathbf{r}_{ij}| \leq r_a\}$  with its size  $|\mathcal{A}_i|$ .

The equation of motion is

$$\begin{aligned} \tau_0 \frac{d\mathbf{v}_i}{dt} = & (v_0 - |\mathbf{v}_i|) \frac{\mathbf{v}_i}{|\mathbf{v}_i|} + \frac{1}{|\mathcal{L}_i|} \sum_{j \in \mathcal{L}_i} g(|\mathbf{r}_{ij}|) (\mathbf{v}_j - \mathbf{v}_i) \\ & + \frac{1}{|\mathcal{L}_i|} \sum_{j \in \mathcal{L}_i} g(|\mathbf{r}_{ij}|) \left( v_r \frac{\mathbf{r}_{ij}}{|\mathbf{r}_{ij}|} - \mathbf{v}_i \right) \\ & + \frac{\Lambda_i(t)}{|\mathcal{A}_i|} \sum_{j \in \mathcal{A}_i} \left( v_a \frac{\mathbf{r}_{ji}}{|\mathbf{r}_{ji}|} - \mathbf{v}_i \right), \end{aligned} \quad (1)$$

where  $\mathbf{r}_{ij} = \mathbf{r}_i - \mathbf{r}_j$ . On the left-hand side, we set the mass of the agent to be unity and introduce the characteristic time-scale  $\tau_0$ . The four terms on the right-hand side represent the self-driving force and the orientational, repulsive, and attractive interactions, respectively. The constants  $v_r$  and  $v_a$  are the speed of collision avoidance and speed of fast-start, respectively. The repulsive and orientational interaction are enhanced due to body con-

tact (excluded volume effect), which we incorporate into the function

$$g(|\mathbf{r}|) = \begin{cases} \frac{r_b}{|\mathbf{r}|} & [|\mathbf{r}| \leq r_b], \\ 1 & [|\mathbf{r}| > r_b], \end{cases} \quad (2)$$

where  $r_b$  is the body length.

We define the dimensionless strength of attraction  $\Lambda_i(t)$  in order to incorporate the screened attractive force in a cluster and the duration of attraction by fast-start. The function  $\Lambda_i(t)$  changes in time depending on the history of the size of  $\mathcal{L}_i(t)$  as follows. The attraction is turned on ( $\Lambda_i(t) = \lambda$ ) at the moment when  $|\mathcal{L}_i(t)|$  becomes smaller than  $N_u$ . The attraction lasts for the duration  $\tau$ . If  $|\mathcal{L}_i(t)| = N_u$  after the period  $\tau$ , the attraction is switched off ( $\Lambda_i(t) = 0$ ). Otherwise, if  $|\mathcal{L}_i(t)| < N_u$  after the first period, the attraction is maintained for another period  $\tau$ , and this will be repeated until we finally get  $|\mathcal{L}_i(t)| = N_u$ ; see FIG. S1(a)-(c) for graphical illustration.

Numerical integration of the equation of motion is carried out by the Runge-Kutta method, and the time step  $dt = 0.005$  is used unless otherwise stated. We rescale all lengths by the radius of equilibrium  $r_e = 1.5$  BL [37, 38] and time by the characteristic timescale  $\tau_0 = 1$  sec, which is estimated from the experiments [49–54]: henceforth  $r_e = 1$  and  $\tau_0 = 1$ . Other parameters are also estimated from the experimental values as  $r_a = 5$ ,  $v_0 = 1$ ,  $v_r = 1$ ,  $v_a = 5$ , and  $\tau = 0.1$ . The interaction capacity  $N_u$  and the strength of attraction  $\lambda$  are treated as adjustable parameters of the model. The numerical simulation is carried out with  $N = 3000$  or 10000 agents and with two types of initial conditions: (i) The agents have randomly distributed positions and directions with the same speed  $v_0$  ( $L = 35, 40$ ). (ii) The agents are randomly distributed in a single spherical cluster with the same direction and speed ( $L = 120$ ). Details of the parameter values and the initial conditions are given in Supplemental Material.

*Cluster Shapes, Phase Diagram, and Scaling Law.* Typical snapshots at dynamically steady states ( $t = 1500$ ) are shown in FIG. 1. The initial condition (i) is used for (a)-(c) and (ii) in (d)-(e). Giant vortices are spontaneously formed by choosing appropriate parameter values. FIG. 1(a)-(b) display giant “tori” whose sizes are larger than  $r_a$ . Shown in FIG. 1(c) is a “rotating ball”, a spherical vortex looking like a “bait-ball” [7, 9]. FIG. 1(d)-(e) show “rings” with holes larger than the interaction range.

To classify the cluster shapes quantitatively, we monitored the outer and inner radii of the cluster, the principal moments of inertia, as well as the orientational and rotational order parameters, all of which converged by the time  $t = 1500$  if the cluster is stable (see Supplemental Material for their definitions and FIG. S4 for time evolution). The clusters are classified into 7 patterns: (i) rotating ball, (ii) torus, (iii) ring, (iv) polarized school, (v) swarm, (vi) splitting, and (vii) undetermined form. (i) A rotating ball is a rotating cluster that is almost spherical and hence has small differences between its principal mo-

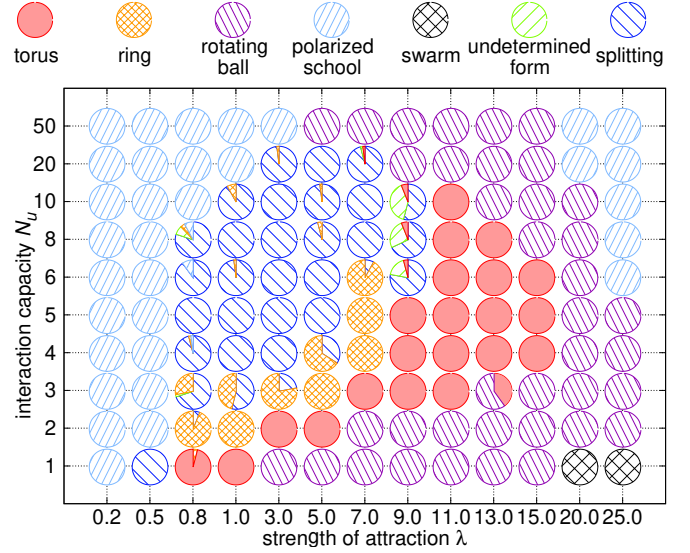


FIG. 2. Phase diagram of the patterns ( $N = 3000$ ) with initial condition (ii). The simulation time is up to  $t = 1500$ . A pie chart shows the frequency of occurrence of each pattern in 50 runs performed for each parameter set  $(\lambda, N_u)$ .

ments of inertia. (ii) A torus is a rotating cluster with a hole at its center (the inner radius  $< r_e$ ). (iii) A ring is a rotating cluster with the inner radius larger than  $r_e$ . (iv) A polarized school is a cluster in which the agents have almost the same direction, and thus the cluster shows directed movement. (v) A swarm is an orientationally disordered cluster in which no characteristic order in the orientation of the agents is observed. (vi) Splitting is a state in which the initial cluster is unstable and is divided into several clusters. (vii) An undetermined form means a single cluster whose shape is constantly changing and the fluctuation of the order parameters are large. (See FIG. S5 for the quantitative definition of these patterns, and FIG. S3 and Movie S6, S8 for the shapes of non-rotating clusters.)

We run the simulation for 50 times for each parameter set  $(\lambda, N_u)$  with  $N = 3000$ , and obtained the phase diagram in FIG. 2. It shows the frequency of occurrence of each pattern by pie charts. Vortex-type clusters (rings, tori, and rotating balls) are obtained in a wide range of parameters, although we used the initial conditions in which the agents are aligned. The vortex-type clusters frequently appear especially for small  $N_u$  and large  $\lambda$ . On the other hand, a polarized school mainly emerges for large  $N_u$  and small  $\lambda$ . Splitting and undetermined form are observed at the transition from a polarized school with small  $\lambda$  to a ring or a torus.

The size of a rotating cluster changes non-monotonically with  $N_u$  with a peak at  $N_u = 2$  or 3 (see FIG. S10(a)), while the size and period of rotation are decreasing functions of  $\lambda$  and increasing functions of  $N$  (see FIG. S11). The average orbital length of each agent is proportional to the average period as shown in FIG. S11(c), and the proportional coefficient gives the aver-



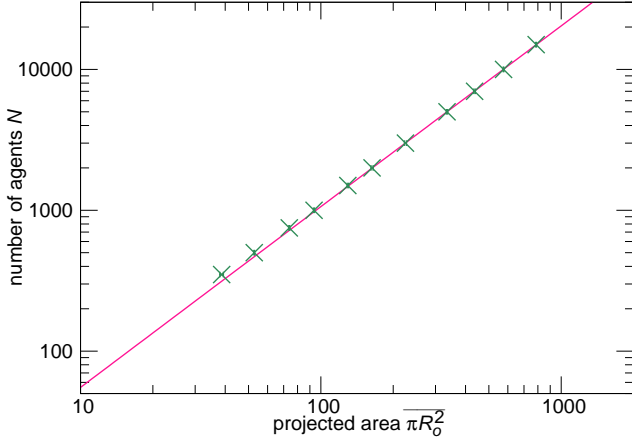


FIG. 3. Scaling relation between projected area  $\overline{\pi R_o^2}$  and the number of agents  $N$  by Log-Log plot ( $N_u = 3, \lambda = 11.0$ ). The green points represent the arithmetic average of the time-averaged  $\pi R_o^2(t)$  obtained in each of the 10 simulations, and the error bars represent the standard deviation. Fitting by the power law  $N \propto (\overline{\pi R_o^2})^\nu$  gives  $\nu = 1.283$  (the magenta line) over the range  $350 \leq N \leq 15000$ .

aged tangential velocity within the cluster  $v = 0.45$ .

In FIG. 3, we plot the number of agents  $N$  versus the projected area of a cluster on the plane perpendicular to the vortex axis for  $N_u = 3, \lambda = 11.0$ . For this parameter set, a rotating cluster without a hole is found over a wide range of  $N$ ; see FIG. S13. Therefore, the projected area is estimated by  $\pi R_o^2$ , where  $R_o$  is the outer radius of the cluster and time average is taken. We find that the size-area relation is well fitted by the scaling law  $N \propto (\pi R_o^2)^\nu$  with  $\nu = 1.283 \pm 0.004$ .

*Motion of Individual Agents.* Next we analyze the orbit of each agent in the cluster. The orbit is projected onto a plane perpendicular to the vortex axis, which is parallel to the total angular momentum of the cluster by definition. FIG. 4 shows time-evolution of the radial distance  $c^\perp$  of a randomly chosen agent and one of its in-plane coordinate  $c_1^\perp = c^\perp \cos \phi$ . From the plot of  $c_1^\perp(t)$ , we see that the agent shows a nearly periodical motion with a period of about  $100\tau_0$ . The plot of  $c^\perp(t)$  shows that the agent moves back and forth between the outer and inner regions of the cluster, and hence the orbit is deviated from a circular trajectory. Although the back-and-forth motion is random, its time-scale is comparable to several orbital periods. To characterize the random motion, we measured the autocorrelation function  $G(\Delta t)$  of the radial distance  $c^\perp(t)$ , where  $\Delta t$  is the time lag. We find that  $G(\Delta t)$  decays more rapidly than exponentially, which means that some disturbance is added to a simple random walk in the radial direction. The disturbance is attributed to the motion of the vortex axis, and is stronger for a cluster with a smaller aspect ratio (radius/height) and hence for larger  $\lambda$ , as demonstrated by Eq. S24 and FIG. S9(a).

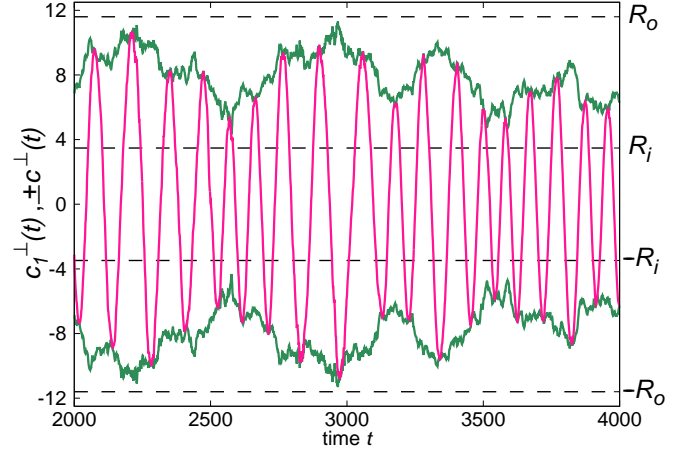


FIG. 4. Time evolution of the radial distance  $c^\perp(t)$  of a certain agent in a ring, and  $c_1^\perp(t) = c^\perp(t) \cos \phi(t)$  where  $\phi(t)$  is the azimuthal angle in the projected plane ( $N = 3000, N_u = 3, \lambda = 4.5$ ). This orbit is obtained from  $t = 2000$  to  $t = 4000$  with the initial condition (ii). The upper green line shows the radial distance  $c^\perp(t)$  between the agent and axis of rotation of the cluster, and the lower green line shows  $-c^\perp(t)$ . The magenta line between the  $\pm c^\perp(t)$  lines shows  $c_1^\perp(t)$ . The dashed lines represent the time averages of the outer radius  $\pm R_o(t)$  and the inner radius  $\pm R_i(t)$  over the same time period.

The number density of agents has a peak at finite radial distance not only for a torus and a ring (which is trivial by definition) but also for a rotating ball; the peak moves toward the center as  $\lambda$  is increased (see FIG. S14). On the other hand, the occupancy ratio is saturated at  $\eta = 1$  except at the surface regions of width  $\sim r_e$ , where the agents are attracted by those inside the cluster (see FIG. S14(a)). We also studied the spatial distribution of the velocity in rotating clusters, and found that it has peaks at the surfaces while it is constant inside the cluster (see FIG. S15).

*Discussion.* We found that giant rotating clusters (torus, ring, and ball) emerge by reducing the interaction capacity  $N_u$ , and without assistance of asymmetrical interaction via a blind angle. Tori [20, 21, 24, 26] and rings [20] are often found in previous 3D models, but their sizes don't exceed the characteristic interaction ranges. Our model exhibits, in addition to a torus and a ring, a giant ball-shaped rotating cluster, which is similar to a “bait-ball” [7, 9], which is almost spherical for  $N_u = 1$  (see FIG. S10(b)). In some models using isotropic potential [19–22], there are parameter regions where either schools or mills appear depending on the initial conditions. In contrast, in our model, stable tori and rotating balls are always found in different parameter regions even though we start from oriented clusters (initial condition (ii)) as shown FIG. 2.

On the other hand, the cluster size decreases as  $N_u$  is increased, and becomes comparable to the radius of interaction for  $N_u = 50$  (see FIG. S10(a)). Therefore, the interaction is almost global when  $N_u = 50$ . We obtained

polarized schools when  $N_u$  is large (see FIG. 2), which is consistent with a previous 3D model without interaction capacity that obtained schools over wide parameter regions [20] (in contrast to a 2D model with the same potential [19]).

In our model, the cluster size is an increasing function of the number of agents (see FIG. S11(a) and FIG. S13(b)). In contrast, in a previous model with an isotropic potential [19], the cluster size decreases as the number of agents increases. This is an essential difference arising from non-additivity due to interaction capacity in our model; attractive forces act on only the agents near the surface of a cluster as shown in FIG. S14(a). Furthermore, the rotational order parameter  $M$  increases monotonically as the number of agents increases (see FIG. S13(a)), unlike [31, 36] where  $M$  reaches its peak at several hundred agents.

The actual size of clusters with 3000 sardines is reported in Ref. [8]: The inner and outer radii of a torus-type cluster is  $1 \sim 2$  BL and  $13 \sim 17$  BL, respectively [55]. These values are close to the radii we obtained for  $N = 3000$ ,  $N_u = 3$ , and  $\lambda = 7.0$ , which are 1 BL (inner radius) and 15 BL (outer radius); see FIG. S10(a).

As for the scaling law of the cluster size, experiments report  $\log(\text{biomass}) = 1.329 \times \log(\text{school area}) + 0.428$  for herring (*Clupea harengus*) and mackerel (*Scomber scombrus*) [56]. The exponent  $\nu = 1.283$  in our model is in good agreement with the experimental value. The exponent should be 1 for a disk of constant thickness and density, while  $\nu = 3/2 = 1.5$  for a sphere of constant density. The experimental and our numerical results show that rotating clusters are intermediate between a disk and a sphere.

In our model, the velocity is almost constant inside the cluster (see FIG. S15), while in the experiment, the velocity increases with the distance from the vortex axis [8]. This could be improved by introducing heterogeneity of swimming velocity, which makes faster agents distributed in the outer side of a cluster [29]. Heterogeneity in other characteristics, such as the blind angle [57], also controls the shape and size of the cluster, and might affect the velocity distribution.

Finally, it is important to reproduce the verticality of the vortex axis in actual fish clusters, which is presumably due to gravity and upward movement of predators near water surface [5, 9]. Inclusion of these effects into the model will be an interesting issue for the future.

- 
- [1] L. Conradt and T.J. Roper, Trends. Ecol. Evol. **20**, 449 (2005).
  - [2] M. Moussaid, S. Garnier, G. Theraulaz, and D. Helbing, Topics in Cognitive Sci. **1**, 469 (2009).
  - [3] T. Vicsek and A. Zafeiris, Physics Reports **517**, 71 (2012).
  - [4] J. Delcourt, N.W.F. Bode, and M. Denoël, Quart. Rev. Biol. **91**, 1 (2016).
  - [5] T. Similä, Aquat. Mamm. **23**, 119 (1997).
  - [6] J.K. Parrish, S.V. Viscido, and D. Grünbaum, Biol. Bull. **202**, 296 (2002).
  - [7] U. Lopez, J. Gautrais, I.D. Couzin, and G. Theraulaz, Interface Focus **2**, 693 (2012).
  - [8] K. Terayama, H. Hioki, and M. Sakagami, Inter. J. Semantic Comput. **9**, 143 (2015).
  - [9] R. Masadeh, B.A. Mahafzah, and A. Sharieh, Int. J. Adv. Comput. Sci. Appl. **10**, 388 (2019).
  - [10] I. H. Riedel, K. Kruse, and J. Howard, Science **309**, 300 (2005).
  - [11] Y. Sumino, K. H. Nagai, Y. Shitaka, D. Tanaka, K. Yoshikawa, H. Chaté, and K. Oiwa, Nature **483**, 448 (2013).
  - [12] H. Wioland, F. G. Woodhouse, J. Dunkel, J. O. Kessler, and R. E. Goldstein, Phys. Rev. Lett. **110**, 268102 (2013).
  - [13] H. Wioland, F. G. Woodhouse, J. Dunkel, and R. E. Goldstein, Nat. Phys. **12**, 341 (2016).
  - [14] K. Tunström, Y. Katz, C. C. Ioannou, C. Huepe, and M. J. Lutz, I. D. Couzin, PLoS Comput. Biol., **9**, e1002915 (2013).
  - [15] I. Aoki, Bull. Jap. Soc. Sci. Fish **48**, 1081 (1982).
  - [16] C. Reynolds, Comput. Graph (ACM) **21**, 25 (1987).
  - [17] H. Niwa, J. theor. Biol. **171**, 123 (1994).
  - [18] T. Vicsek, A. Czirók, E. Ben-Jacob, I. Cohen, and O. Shochet, Phys. Rev. Lett. **75**, 1226 (1995).
  - [19] M.R. D’Orsogna, Y.L. Chuang, A.L. Bertozzi, and L.S. Chayes, Phys. Rev. Lett. **96**, 104302 (2006).
  - [20] N.H.P. Nguyen, E. Jankowski, and S.C. Glotzer, Phys. Rev. E **86**, 011136 (2012).
  - [21] Y.L. Chuang, T. Chou, and M.R. D’Orsogna, Phys. Rev. E **93**, 043112 (2016).
  - [22] Z. Cheng, Z. Chen, T. Vicsek, D. Chen, and H.T. Zhang, New J. Phys. **18**, 103005 (2016).
  - [23] N. Shimoyama, K. Sugawara, T. Mizuguchi, Y. Hayakawa, and M. Sano, Phys. Rev. Lett. **76**, 3870 (1996).
  - [24] I.D. Couzin, J. Krause, R. James, G.D. Ruxton, and N.R. Franks, J. theor. Biol. **218**, 1 (2002).
  - [25] D. Strömbom, J. theor. Biol. **283**, 145 (2011).
  - [26] D. Strömbom, M. Siljestam, J. Park, and D.J.T. Sumpter, Eur. Phys. J. Spec. Top. **224**, 3311 (2015).
  - [27] L. Barberis and F. Peruani, Phys. Rev. Lett. **117**, 248001 (2016).
  - [28] A. Costanzo and C.K. Hemelrijk, J. Phys. D: Appl. Phys. **51**, 134004 (2018).
  - [29] A. Costanzo, Europhys. Lett. **125**, 20008 (2019).
  - [30] For an attempt to apply the idea of topological interaction to fish, see: J. Gautrais, F. Ginelli, R. Fournier, S. Blanco, M. Soria, H. Chaté, and G. Theraulaz, PLoS Comput. Biol. **8**, e1002678 (2012).
  - [31] D.S. Calovi, U. Lopez, S. Ngo, C. Sire, H. Chaté, and G. Theraulaz, New J. Phys. **16**, 015026 (2014).
  - [32] M. Ballerini, N. Cabibbo, R. Candelier, A. Cavagna, E. Cisbani, I. Giardina, V. Lecomte, A. Orlandi, G. Parisi, A. Procaccini, M. Viale, and V. Zdravkovic, Proc. Natl. Acad. Sci. U.S.A. **105**, 1232 (2007).

- [33] A. Cavagna, A. Cimorelli, I. Giardina, G. Parisi, R. Santagati, F. Stefanini, and M. Viale, *Proc. Natl. Acad. Sci. U.S.A.* **107**, 11865 (2009).
- [34] N.W.F. Bode, D.W. Franks, and A.J. Wood, *J. R. Soc. Interface* **8**, 301 (2011).
- [35] W. Bialek, A. Cavagna, J. Giardina, T. Morad, E. Silvestri, M. Viale, and A.M. Walczak, *Proc. Natl. Acad. Sci. U.S.A.* **109**, 4786 (2012).
- [36] A. Filella, F. Nadal, C. Sire, E. Kanso, and C. Eloy, *Phys. Rev. Lett.* **120**, 198101 (2018).
- [37] Y. Katz, K. Tunström, C.C. Ioannou, C. Huepe, and I.D. Couzin, *Proc. Natl. Acad. Sci. U.S.A.* **108**, 18720 (2011).
- [38] J.E. Herbert-Read, A. Perna, R.P. Mann, T.M. Schaerf, D.J.T. Sumpter, and A.J.W. Ward, *Proc. Natl. Acad. Sci. U.S.A.* **108**, 18726 (2011).
- [39] B.L. Partridge, T. Pitcher, J.M. Cullen, and J. Wilson, *Behav. Ecol. Sociobiol.* **6**, 277 (1980).
- [40] B.C. Jayne and G.V. Lauder, *J. Comp. Physiol. A* **173**, 495 (1993).
- [41] I.L.Y. Spierts and J.L. van Leeuwen, *J. Exp. Biol.* **202**, 393 (1999).
- [42] J.M. Wakeling, in *Fish Physiology*, edited by R.E. Shadwick and G.V. Lauder (Elsevier Academic Press, London, 2006), p. 333.
- [43] J.R. Hunter, *Anim. Behav.* **17**, 507 (1969).
- [44] D. Radakov, *Schooling in the ecology of fish* (Wiley, New York, 1973).
- [45] J. Godin and M.J. Morgan, *Behav. Ecol. Sociobiol.* **16**, 105 (1985).
- [46] P.W. Webb, *J. Exp. Biol.* **74**, 211 (1978).
- [47] P. Domenici and R.W. Blake, *J. Exp. Biol.* **200**, 1165 (1997).
- [48] D.S. Calovi, A. Litchinko, V. Lecheval, U. Lopez, A.P. Escudero, H. Chaté, C. Sire, and G. Theraulaz, *PLoS Comput. Biol.* **14**, e1005933 (2018).
- [49] T.Y. Wu, in *Scale Effects in Animal Locomotion*, edited by T.J. Pedley (Academic Press, London/New York, 1977), p. 203.
- [50] J.J. Videler and C.S. Wardle, *Rev. Fish Biol. Fish* **1**, 23 (1991).
- [51] G.V. Lauder and E.D. Tytell, in *Fish Physiology*, edited by R.E. Shadwick and G.V. Lauder (Elsevier Academic Press, London, 2006), p. 425.
- [52] C. Katopodis and R. Gervais, *River Res. Applic.* **28**, 444 (2012).
- [53] E.D. Tytell, *Proc. R. Soc. Lond. B* **271**, 2535 (2004).
- [54] T.N. Wise, M.A.B. Schwalbe, and E.D. Tytell, *J. Exp. Biol.* **221**, jeb190892 (2018).
- [55] We use Fig. 8 (a-b) and (e-f) in Ref. [8] as datas for comparison.
- [56] O. A. Misund, *Aquat. Living Resour.* **6**, 235 (1993).
- [57] W. L. Romey and J. M. Vidal, *Ecol. Model.* **258**, 9 (2013).